Top-down estimates of benzene and toluene emissions in the Pearl River Delta and Hong Kong, China

Xuekun Fang[1], Min Shao[2], Andreas Stohl[3], Qiang Zhang[4], Junyu Zheng[5], Hai Guo[6], Chen Wang[2,7], Ming Wang[2], Jiamin Ou[8], Rona L. Thompson[3], and Ronald G. Prinn[1]

[1]Center for Global Change Science, Massachusetts Institute of Technology, Cambridge, Massachusetts, USA
[2]State Key Joint Laboratory of Environmental Simulation and Pollution Control, College of Environmental Sciences and Engineering, Peking University, Beijing, China
[3]Norwegian Institute for Air Research, Kjeller, Norway
[4]Ministry of Education Key Laboratory for Earth System Modeling, Center for Earth System Science, Tsinghua University, Beijing, China
[5]College of Environment and Energy, South China University of Technology, University Town, Guangzhou, China
[6]Air Quality Studies, Department of Civil and Environmental Engineering, The Hong Kong Polytechnic University, Hong Kong, China
[7]College of Environmental Engineering and Science, Qilu University of Technology, Jinan, Shandong, China
[8]Institute of Space and Earth Information Science, The Chinese University of Hong Kong, Hong Kong, China

Correspondence to: Xuekun Fang (fangxk@mit.edu) and Min Shao (mshao@pku.edu.cn)

Abstract. Benzene (C_6H_6) and toluene (C_7H_8) are toxic to humans and the environment. They are also important precursors of ground-level ozone and secondary organic aerosols and contribute substantially to severe air pollution in urban areas in China. Discrepancies exist between different bottom-up inventories for benzene and toluene emissions in the Pearl River Delta (PRD) and Hong Kong (HK), which are emission hot spots in China. This study provides top-down estimates of benzene and toluene emissions in the PRD and HK using atmospheric measurement data from a rural site in the area, Heshan, an atmospheric transport model, and an inverse modeling method. The model simulations captured the measured mixing ratios during most pollution episodes. For the PRD and HK, the benzene emissions estimated in this study for 2010 were $44\,(12–75)$ and $5\,(2–7)\,\mathrm{Gg\,yr^{-1}}$ for the PRD and HK, respectively, and the toluene emissions were $131\,(44–218)$ and $6\,(2–9)\,\mathrm{Gg\,yr^{-1}}$, respectively. Temporal and spatial differences between the inversion estimate and four different bottom-up emission estimates are discussed, and it is proposed that more observations at different sites are urgently needed to better constrain benzene and toluene (and other air pollutant) emissions in the PRD and HK in the future.

1 Introduction

Benzene and toluene, two volatile organic compounds (VOCs), are toxic to humans and the environment. For example, a sufficiently high exposure of toluene will lead to health issues like intra-uterine growth retardation, premature delivery, congenital malformations, and postnatal developmental retardation (Donald et al., 1991). VOCs, including benzene and toluene, are also important precursors of ground-level ozone, which is produced from the reaction between VOCs and NO_x in the presence of sunlight (Xue et al., 2014), and contribute to the formation of secondary organic aerosols (Henze et al., 2008). VOCs emitted from anthropogenic activities are important contributors to severe urban haze pollution in China (Guo et al., 2014). Therefore, information about the spatial and temporal distribution of benzene and toluene emissions is crucial for air quality

simulations and predictions, health risk assessments, and emission control policy.

The Pearl River Delta (PRD) and Hong Kong (HK) are located along the coast of southern China, which is one of the most economically developed areas in the country. It is also where the densely populated mega-cities, Guangzhou and Shenzhen (in the PRD) and Hong Kong are located. The PRD and HK regions experience severe air pollution, namely toxic trace gases and particulates, as observed by satellites (e.g., van Donkelaar et al., 2010) and ground-based measurements (e.g., Guo et al., 2009). Toluene and benzene were found to be two of the most abundant VOCs in the PRD (Chan et al., 2006). Toluene and benzene, respectively, had the largest and second largest emissions of all anthropogenic VOCs in the PRD in 2010 (Ou et al., 2015), which highlights the importance of accurately quantifying these emissions. In the PRD, the two major sources of benzene are industrial processes and road transport, and those of toluene are industrial solvents and road transport, while minor sources for both benzene and toluene include stationary combustion, gasoline evaporation, biomass burning, etc. (Ou et al., 2015).

Although some bottom-up inventories exist for benzene and toluene emissions in the PRD, there are discrepancies among them. For example, for benzene emissions in 2010, the Regional Emission inventory in Asia (REAS) v1.1 reference scenario (from here on referred to as REAS REF v1.1) estimates the emissions to be $8\,Gg\,yr^{-1}$ (Ohara et al., 2007), while the Multi-resolution Emission Inventory (MEIC) v1.2 (available at http://www.meicmodel.org) estimate is $33\,Gg\,yr^{-1}$, the Representative Concentration Pathways Scenario 2.6 (RCP2.6) estimate is $45\,Gg\,yr^{-1}$ (van Vuuren et al., 2007), and the Yin et al. (2015) estimate is $54\,Gg\,yr^{-1}$. Thus, estimates of the total emissions vary by a factor of approximately seven. For toluene emissions in 2010, the estimates are also quite different: The RCP2.6 and REAS v1.1 REF estimates are 44 and $46\,Gg\,yr^{-1}$, respectively, the Yin et al. (2015) estimate is $64\,Gg\,yr^{-1}$, and the MEIC v1.2 estimate is $181\,Gg\,yr^{-1}$. Atmospheric-measurement-based estimates are needed to validate benzene and toluene emissions estimated from bottom-up methods. However, to date no top-down estimate is available for the PRD and HK.

High-frequency online measurements of VOCs (including benzene and toluene) were made during the PRIDE-PRD2010 Campaign (Program of Regional Integrated Experiments on Air Quality over Pearl River Delta) during November and December 2010. This study uses these measurement data and an inverse modeling approach to infer benzene and toluene emissions in the PRD and HK. This top-down estimate is important to test and improve the existing bottom-up inventories.
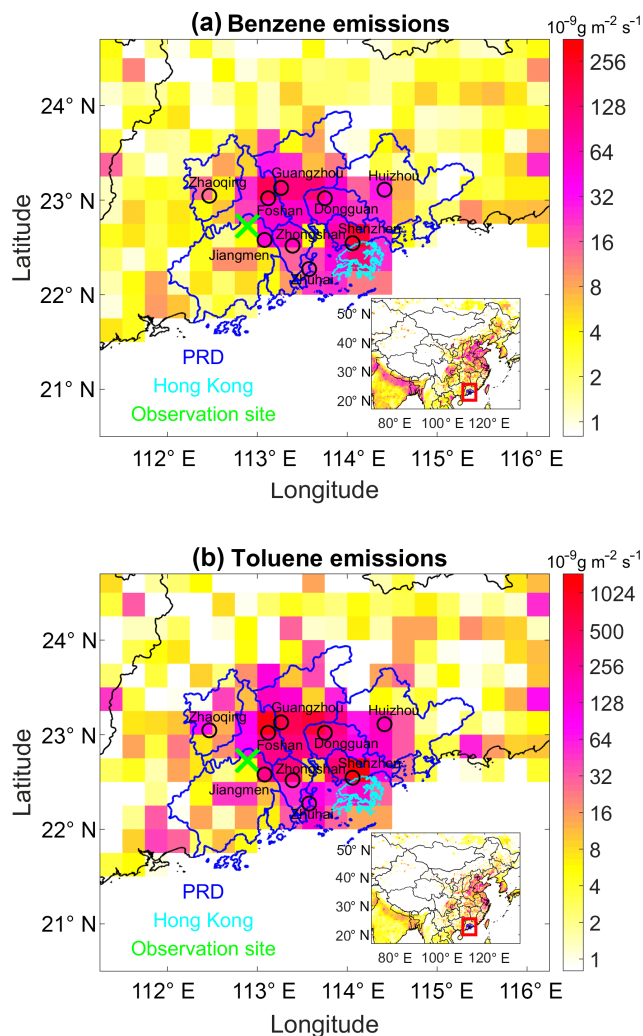
Figure 1. Map of **(a)** benzene and **(b)** toluene emissions from the MEIC v1.2 for China and the RCP2.6 for outside China (inset), and that for the PRD and Hong Kong regions (main panels). The PRD region is plotted with dark blue boundary lines, the Hong Kong region with cyan boundary lines. The green cross indicates the location of the Heshan observation site. The hollow black circle indicates the location of the major cities in the PRD.

2 Methodology

2.1 Measurement data

In this study, atmospheric measurements of benzene and toluene at two sites were used: the Heshan site (used for the inversion) and the Tai Mo Shan (TMS) site (used for validation). The Heshan site (112.929° E, 22.728° N) is a rural observatory located on the top of a small hill ($\sim 60\,m$ above the surrounding terrain; $\sim 100\,m$ a.s.l. – above sea level) in Jiangmen (see Fig. 1). The measurement period at the Heshan site was from 11 November to 1 December 2010. Data from 1 December 2010 were not used, since we focused

on mixing ratios and emissions in November. Detailed information of the measurement system and procedure can be found in Wang et al. (2014). Here we provide only a brief description. Ambient mixing ratios of VOCs were measured using an online automatic gas chromatograph system equipped with a mass spectrometer and a flame ionization detector (GC-MS/FID). Most C_2–C_5 hydrocarbons were measured by the FID Channel with a porous layer open tubular (PLOT) column, whereas other VOCs, including benzene and toluene, were measured by the Mass Selective Detector (MSD) Channel with a DB-624 column. The time resolution of the VOC measurements was 60 min. The detection limits of this system for benzene and toluene are 0.006 and 0.015 ppb, respectively, which are much lower values than the typical benzene and toluene mixing ratio levels of 2 and 6 ppb during the observation period at the Heshan site.

The TMS site (114.118° E, 22.405° N) was not used for the inversion but for validating the emissions derived from the inversions in this study. The sample air inlet at the TMS site was located on the rooftop of a building at TMS at an elevation of 640 m a.s.l. level. A total of 75 canisters of air samples were taken over different times of day and night on 1–3, 9, and 19–21 November 2010. Detailed information on the sampling time schedule can be found in Guo et al. (2013). After sampling, the VOC canister samples were sent to a laboratory at the University of California, Irvine for chemical analysis. Simpson et al. (2010) provide a full description of the analytical system, which uses a multi-column gas chromatograph (GC) with five column-detector combinations. The measurement detection limit of this system for both benzene and toluene is 0.003 ppb, which is much lower than the typical mixing ratio levels of 0.7 ppb for benzene and 1.6 ppb for toluene during the observation period at the TMS site.

The TMS data were not used in the inversion because: (1) the measurements performed at the two stations were calibrated according to different scales, which may cause problems in the inversion (see also Weiss and Prinn, 2011); (2) the number of measurement data at the TMS site (totally 75 in November 2010) is much smaller than that at the Heshan site (totally 419), which means that the inversion results would anyway be dominated by the Heshan data; (3) TMS is relatively close to central Urban Hong Kong ($\sim$ 7 km; Guo et al., 2013) so that the TMS site might be influenced by local sources and this is not desirable for the inversion. Tests with inversions including TMS data have shown that the PRD benzene emissions would be only $\sim$ 15 % higher from those using Heshan data only, which is within the a posteriori emission uncertainty.

2.2 Model simulations using FLEXPART

The source–receptor relationships (SRRs, often also called "emission sensitivities", in units of m^2 s g^{-1}) were calculated using the backwards-in-time mode of the Lagrangian particle dispersion model, FLEXPART (http://www.flexpart.eu) (Stohl et al., 1998, 2005). The model was driven by hourly meteorological data of 0.5° × 0.5° horizontal resolution and 37 vertical levels from the NCEP Climate Forecast System Reanalysis (CFSR) (available at http://rda.ucar.edu/datasets/ds093.0/) (Saha et al., 2010). During 3-hourly intervals throughout the sampling period, 80 000 virtual particles were released at the site's location and at the height of the sampling inlet above model ground level, and followed backwards in time for 20 days. In FLEXPART, the trajectories of tracer particles are calculated using the mean winds interpolated from the analysis fields plus random motions representing turbulence (Stohl and Thomson, 1999). The emission sensitivity value in a particular grid cell is proportional to the particle residence time in that cell (Seibert and Frank, 2004). Residence time is specifically for the layer from the surface up to a specified height in the planetary boundary layer (100 m used by this study and previous studies, e.g., Stohl et al., 2009). The spatial resolution of the output from the backward simulations is 0.25° × 0.25°. Loss of benzene and toluene by reaction with the hydroxyl (OH) radical in the atmosphere was considered in the backward simulation. Rate constant values for reaction with OH radicals were expressed for benzene as

$$k = 2.308 \times 10^{-12} \times \exp\left(-\frac{190}{T}\right) \qquad (1)$$

and for toluene as

$$k = 1.275 \times 10^{-18} \times T^2 \times \exp\left(\frac{1192}{T}\right), \qquad (2)$$

where T is the ambient temperature (K). Gridded OH fields (hourly for the period October to December 2010, at a resolution of 0.5° × 0.667°, 47 vertical levels) were derived from the atmospheric chemistry transport model, GEOS-Chem v5 (http://acmg.seas.harvard.edu/geos/). A reference simulation was run backwards for 20 days with atmospheric chemical loss, and additional alternative FLEXPART simulations were run backwards for 10 and 40 days with atmospheric chemical loss, and 20 days without atmospheric chemical loss (see Sect. 3.2).

2.3 Inverse algorithm

Simulated benzene and toluene mixing ratios at the measurement site were obtained by integrating the gridded emission sensitivities (m^2 s g^{-1}) multiplied by the gridded emissions (g m^{-2} s^{-1}). The Bayesian inversion method used in this study is almost the same as described and evaluated by Stohl et al. (2009, 2010), and as used in recent studies of SF$_6$ emissions (Fang et al., 2014) and HFC-23 emissions (Fang et al., 2015) in East Asia. Briefly, in this study a Bayesian inversion technique is employed, based on least-squares optimization, to estimate both the spatial distribution and strength of the emissions in the domain over which the

measurements are sensitive. The inversion adjusts the emissions to minimize the differences between the observed and modeled mixing ratios while also considering the deviation of the optimized emissions from an a priori emission field. Uncertainties in the observation space (which include transport model errors) were determined as the root mean square error (RMSE) of the model–observation mismatch (Stohl et al., 2009, 2010). In this study, background mixing ratio values were set to zero. This is because the backward simulations were run for 20 days and benzene and toluene in the air parcel from emissions occurring prior to this time have been largely removed from the atmosphere by reaction with OH (typical atmospheric lifetimes of benzene and toluene are ~ 10 and ~ 2 days, respectively).

For benzene, gridded a priori emission fields for mainland China were derived from MEIC v1.2 for November 2010 ($0.25° \times 0.25°$, monthly mean), and for the rest of the world the emissions were taken from RCP Scenario 2.6 ($0.5° \times 0.5°$, annual mean) (van Vuuren et al., 2007). For toluene, a priori emission fields for mainland China were derived from MEIC v1.2 for November 2010 ($0.25° \times 0.25°$, monthly mean), while for the PRD region in mainland China, a priori emissions were derived by averaging the estimates from MEIC v1.2 ($0.25° \times 0.25°$, monthly mean) and from Yin et al. (2015) ($0.25° \times 0.25°$, monthly mean) for November 2010. For the rest of the world, a priori emissions were taken from RCP2.6 inventory ($0.5° \times 0.5°$, yearly mean) (van Vuuren et al., 2007). Both monthly inventories of MEIC v1.2 and Yin et al. (2015) were obtained through personal communication with the authors of the data set. Tests show that the difference between toluene a posteriori emissions for the PRD from inversions using the averaged MEIC v1.2 and Yin et al. (2015) versus the MEIC v1.2 or Yin et al. (2015), is less than 15 %. The difference of benzene a posteriori emissions from inversions is about 10 % using different benzene a priori emissions. Thus, the choice of a priori emissions does not greatly influence the results. The a priori uncertainty was determined by looking at the differences among bottom-up estimates for each species. For benzene, our a priori emission was 3.1 Gg month^{-1}, compared to 3.7 Gg month^{-1} from RCP2.6, and 4.9 Gg month^{-1} from Yin et al. (2015) for November, and 0.7 Gg month^{-1} from REAS v1.1. Thus, the largest difference with respect to our prior is $1 - 0.7/3.1 = 0.78$, so we set the a priori uncertainty to be 100 %. A posteriori emissions for the PRD from the inversion using 80 % for the benzene uncertainty were only 2.7 % smaller than those from the inversion using 100 %, indicating that the choice of 80 % versus 100 % uncertainty does not have a significant influence on the results. For toluene, our a priori emission was 11.5 Gg month^{-1}, compared to 3.6 Gg month^{-1} from RCP2.6, 5.6 Gg month^{-1} from Yin et al. (2015) for November, 3.8 Gg month^{-1} from REAS v1.1, and 17.4 Gg month^{-1} from MEIC v1.2. Thus, the largest deviation is $1 - 3.6/11.5 = 0.69$, so we set the a priori uncertainty to be 70 %. The a posteriori uncertainty of the emis-

sions in each grid cell was calculated as described by Seibert et al. (2011), and the uncertainty reduction in each grid cell represents the difference (as a percentage) between the a posteriori and a priori emission uncertainties in the corresponding grid cell.

3   Results and discussion

3.1   Benzene and toluene ambient mixing ratios

Table 1 shows ambient mixing ratios of benzene and toluene measured at the Heshan site and other sites all over the world. Mixing ratios of benzene at the Heshan site ranged from 0.59 to 20.23 ppb and had an average of 2.27 ± 1.65 (mean $\pm$ standard deviation) ppb during our observation period. Mixing ratios of toluene at the Heshan site ranged from 0.87 to 25.05 ppb and had an average of 5.65 ± 4.15 ppb. The mixing ratios of benzene (0.67 ± 0.21 ppb) and toluene (1.58 ± 1.25 ppb) at the TMS site were only ~ 30 % of those at the Heshan site. In agreement with previous studies (e.g., Lau et al., 2010; Liu et al., 2008), mixing ratio levels of benzene and toluene in the PRD region are overall higher than those in Hong Kong (Table 1), which is in part due to the fact that Hong Kong often receives clean air masses from over the ocean and that emissions in Hong Kong are lower than in the PRD.

Mixing ratios of benzene and toluene in some cities in Europe (e.g., Ait-Helal et al., 2014; Langford et al., 2010) and the US (e.g., Seila et al., 1989; Baker et al., 2008) have been found to be approximately 0.5 and 1 ppb (Table 1), respectively, which is about 20 % of the mean observed values in the PRD in this study. Mixing ratios of benzene and toluene in Thompson Farm, United States were even 0.08 ± 0.002 and 0.09 ± 0.005 ppb, respectively, which are much lower than the lowest mixing ratios at both Heshan and TMS sites. Levels of benzene and toluene mixing ratios at different sites mainly reflect the combined influence of emission strength, seasonal changes in atmospheric OH concentration, and mixing depth.

3.2   Benzene and toluene emission sensitivities

The meteorological reanalysis CFSR data were compared with measurement data from ground stations. We choose ground stations within the domain (111.45–118.15° E, 21.70–27.33° N) over which the meteorology most likely has the strongest influence on the simulation for the Heshan site. Measurement data are available at 3-hourly intervals from 34 ground stations for the period 1–30 November 2010 (see the station information in Table S1 and the map of stations in Fig. S1 in the Supplement). The mean wind speed at 10 m a.g.l. (above ground level) was 2.4 m s^{-1} in the CFSR data compared to the observed wind speed of 2.2 m s^{-1}. The mean air temperature at 2 m above ground level was 16.1° in the CFSR data compared to the observed temperature of

Table 1. Ambient mixing ratios (ppb) of benzene and toluene measured at the Heshan site and other sites all over the world (SD represents standard deviation; NG indicates not given).

Location	Type	Time	Benzene			Toluene			Reference
			Sample number	Range	Mean ± SD	Sample number	Range	Mean ± SD	
(1) PRD and Hong Kong regions, China									
Heshan, PRD	Rural	11–30 Nov 2010	419	0.59–20.23	2.27 ± 1.65	419	0.87–25.05	5.65 ± 4.15	This study
Guangzhou, PRD	Urban	4 Oct to 3 Nov 2004	111	0.66–11.35	2.39 ± 1.99	111	0.76–36.91	7.01 ± 7.33	Liu et al. (2008)
Xinken, PRD	Rural	4 Oct to 3 Nov 2004	83	0.52–6.26	1.42 ± 0.98	83	0.54–56.41	8.46 ± 9.94	Liu et al. (2008)
Dongguan, PRD	Urban	Sep 2005	48	0.27–6.45	1.26 ± 0.14	48	0.53–25.30	6.13 ± 0.81	Barletta et al. (2008)
Guangzhou, PRD	Urban	Sep 2006	42	0.65–6.80	2.05 ± 1.49	42	0.72–19.60	5.87 ± 4.11	Barletta et al. (2008)
Industrial Area, PRD	Industrial	Late summer 2000	15	NG	2.80 ± 1.70	15	NG	13.5 ± 11.8	Chan et al. (2006)
Tai Mo Shan, Hong Kong	Mountain	1–3, 9, 19–21 Nov 2010	75	0.38–1.79	0.67 ± 0.21	75	0.26–6.30	1.58 ± 1.25	This study
Tap Mun, Hong Kong	Rural	Nov 2006 to Oct 2007	39	0.05–1.67	0.56 ± 0.41	39	0.15–7.12	1.61 ± 1.55	Lau et al. (2010)
Central West, Hong Kong	Urban	Nov 2006 to Oct 2007	40	0.05–1.91	0.60 ± 0.50	40	0.28–8.81	2.64 ± 2.07	Lau et al. (2010)
(2) Other sites in China									
43 cities, China	Urban	Jan–Feb 2001	158	0.7–10.4	NG	158	0.4–11.2	NG	Barletta et al. (2005)
Beijing, China	Urban	Aug 2005	1046	NG	3.03 ± 1.72	1039	NG	1.76 ± 0.89	Song et al. (2007)
Shanghai, China	Urban	15 Jun 2006 to 14 Jun 2007	~365	NG	6.07 ± 11.70	~365	NG	32.80 ± 21.60	Ran et al. (2009)
(3) Sites in other countries									
Karachi, Pakistan	Urban	Winter of 1998–1999	78	0.34–19.3	5.20 ± 4.50	78	0.19–37.0	7.10 ± 7.60	Barletta et al. (2002)
Tokyo, Japan	Urban	Summer 2007	50	NG	0.78 ± 0.61	50	NG	2.14 ± 0.99	Yoshino et al. (2012)
Tokyo, Japan	Urban	Winter 2007	16	NG	0.82 ± 0.28	16	NG	10.10 ± 5.23	Yoshino et al. (2012)
London, UK	Urban	Oct 2010	601	NG	0.15 ± 0.11	589	NG	0.68 ± 0.57	Langford et al. (2010)
Paris, France	Suburban	15 Jan–15 Feb 2010	246	NG	0.32 ± 0.16	246	NG	0.32 ± 0.22	Ait-Helal et al. (2014)
Mexico City, Mexico	Urban	Feb 2002 and Apr–May 2003	~115	NG	3.17 ± 1.75	~86	NG	13.5 ± 9.33	Velasco et al. (2007)
Mexico City, Mexico	Rural	Feb 2002 and Apr–May 2003	~115	NG	0.80 ± 0.91	~86	NG	1.89 ± 1.92	Velasco et al. (2007)
39 cities, USA	Urban	Jun–Sep 1984–1986	835	0.001–0.27	NG	836	0.003–1.30	NG	Seila et al. (1989)
28 cities, USA	Urban	Summer 1999–2005	530	(0.06 ± 0.024)–(0.48 ± 0.24)*	NG	530	(0.12 ± 0.055)–(1.54 ± 0.88)*	NG	Baker et al. (2008)
Thompson Farm, USA	Rural	Fall 2004–2006	201	NG	0.08 ± 0.002	201	NG	0.09 ± 0.005	White et al. (2009)

* This represents the range between the minimal mean value (the corresponding standard deviation) in one of 28 cities and the maximal mean value (the corresponding standard deviation) in another city.

17.5°. Thus, the CFSR meteorological data do not differ much from the ground observations. As examples, time series of wind speed and air temperature in November 2010 at three stations are shown in Figs. S2 and S3, respectively.

Figure 2 shows the spatial distribution of average emission sensitivity of benzene and toluene for the Heshan site for 12–30 November 2010. During the observation period, air masses transported to the Heshan site mainly came from easterly and northerly directions. Considering that the major emission sources in the PRD are located to the east of the Heshan site (Fig. 1), this measurement location is ideally situated for constraining emissions from this region for this period and, as the emission sensitivities show, PRD, HK, and neighboring regions are relatively well constrained by the observations at the Heshan site. Benzene and toluene emissions in the PRD and HK are much higher than emissions in neighboring regions (Fig. 1) and, consequently, the overall mixing ratio contributions (the integral of the emission sensitivities multiplied by emissions) from PRD and HK to the observation site comprise more than 80 % of the total simulated mixing ratios. Note that the emission sensitivities for benzene and toluene are different because there are differences in the chemical loss of these two compounds during atmospheric transport and in the molecular weight. Specifically, the emission sensitivities for toluene are spatially more confined because of its shorter lifetime.

As a sensitivity study, alternative simulations in which FLEXPART was ran backwards for 10 days were made. The derived emission sensitivities are almost identical to the reference simulations with 20 days duration (Supporting Information Fig. S4 for benzene and Fig. S5 for toluene), confirming that 20-day-backward simulations are sufficiently long to account for all benzene and toluene emission sources that can influence the mixing ratios at the Heshan site. Since the lifetime of benzene is ∼ 10 days (much longer than that of toluene), we also made a 40-day-backward simulation from which the emission sensitivities for benzene are also almost identical to the reference simulation of 20 days (Fig. S6). Without accounting for the loss by reaction with OH in the atmosphere, the emission sensitivities for benzene would only be a little higher (by ∼ 10 % in central PRD) (Fig. S7). On the other hand, the emission sensitivities for toluene would be much higher (by ∼ 50 % in central PRD) (Fig. S8). This indicates that accounting for chemical loss has a relatively small effect for simulating benzene mixing ratios at Heshan, whereas it has a profound effect on toluene mixing ratios. Thus, errors in the retrieved emissions due to errors in chemical loss are marginal for benzene but could be significant for toluene.
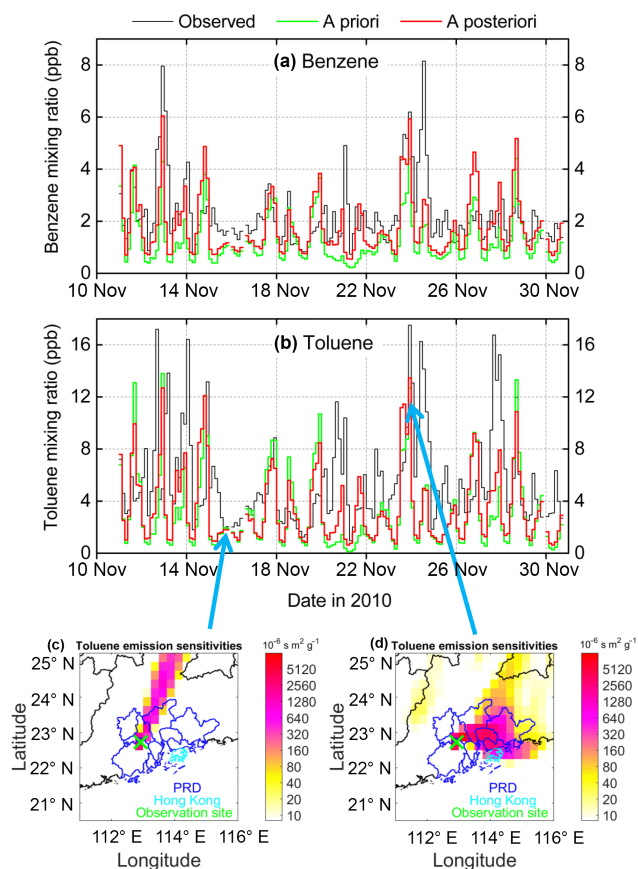
3.3   Inversion results

Figure 3 shows the observed and simulated mixing ratios at the Heshan site. The simulations captured most pollution episodes and the inversion improved the agreement between
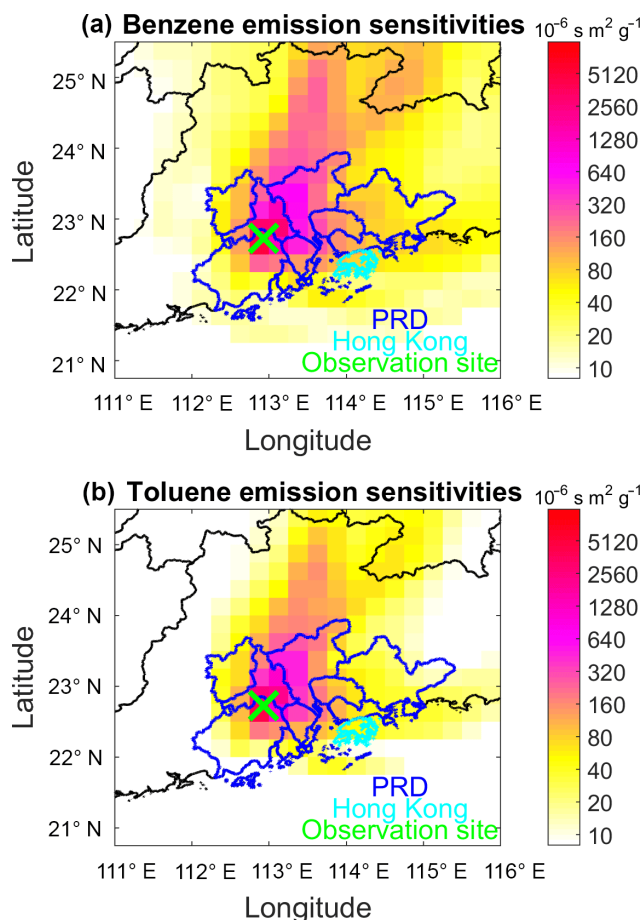
Figure 2. Average emission sensitivities of **(a)** benzene and **(b)** toluene for the Heshan observation site for 12–31 November 2010. The green cross indicates the location of Heshan site. The blue and cyan lines represent PRD and Hong Kong boundary lines, respectively.

the simulations and the observations as expected (the agreement between the a posteriori simulations and the observations is better than for the a priori simulations and the observations). For benzene, the RMSE between the observed and simulated mixing ratios decreased from 1.53 ppb, using a priori emissions, to 1.26 ppb, using a posteriori emissions, and the mean bias between the simulated mixing ratios and observations decreased from 0.96 ppb, using a priori emissions, to 0.41 ppb, using a posteriori emissions. For toluene, the RMSE between the observed and simulated mixing ratios decreased from 4.77 ppb, using a priori emissions, to 4.30 ppb, using a posteriori emissions and the mean bias between the observed and simulated mixing ratios decreased from 2.35 ppb, using a priori emissions, to 1.99 ppb, using a posteriori emissions.

Figure 3 also shows examples of spatial distributions of toluene emission sensitivities for two observed mixing ratios. The toluene mixing ratio at 00:00 UTC on 16 November 2010 was about 2 ppb and the corresponding air mass had

Figure 3. Observed and simulated **(a)** benzene and **(b)** toluene mixing ratios at the Heshan site, and two examples of spatial distributions of toluene emission sensitivities at **(c)** 00:00 UTC on 16 November 2010 and **(d)** 00:00 UTC on 24 November 2010.

Table 2. Benzene and toluene emissions ($Gg\,yr^{-1}$) in the PRD and HK regions derived from different estimates for the year 2010.

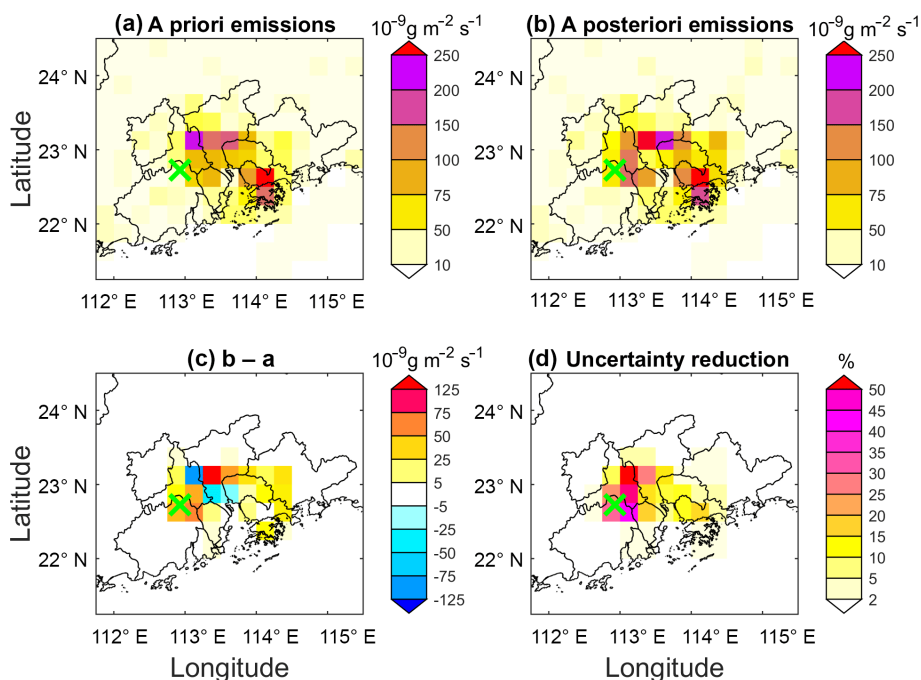| Estimate	Benzene emissions		Toluene emissions	
	PRD	HK	PRD	HK
RCP2.6	45	3	44	4
Yin et al. (2015)	54	NE*	64	NE*
REAS v1.1 REF	8	0.4	46	4
MEIC v1.2	33	NE*	181	NE*
This study	44 (12–75)	5 (2–7)	131 (44–218)	6 (2–9)

* NE indicates "not estimated".

emission in this grid cell was still found, as in the reference inversion.

Figure 5 shows the a priori and a posteriori emissions of toluene and their difference. Emission hot spots are located in Guangzhou and Shenzhen. The uncertainty reduction map in Figs. 4d and 5d shows significant error reductions, of 40 % or more, in boxes close to the observation site, while only low emission uncertainty reductions were achieved in boxes far from the observation site. Overall, the emission uncertainties have been reduced by the inversion in the PRD and HK, where the strongest emission sources are located.

The total a posteriori benzene emissions for PRD and HK, respectively, are 4.0 (1.1–6.9) and 0.4 (0.1–0.7) $Gg\,month^{-1}$. A posteriori toluene emissions are 12 (4–20) $Gg\,month^{-1}$ for PRD and 0.5 (0.2–0.9) $Gg\,month^{-1}$ for HK. The inversion sensitivity tests – i.e., using other bottom-up emission inventories for the a priori estimate (listed in Table 2) – all produce toluene emission estimates that fall within the uncertainty range of the a posteriori emissions from the reference inversion.

Benzene and toluene measurement data at the TMS site were not used in the inversion but for validating the posterior emissions. For benzene, using the a priori and a posteriori emission fields, respectively, the RMSE between the simulated and observed mixing ratios at the TMS site are 0.367 and 0.312 ppb, and the mean bias between the simulated and observed mixing ratios are 0.314 and 0.208 ppb. For toluene, the RMSE (1.50 ppb) between the observed and simulated mixing ratios using the a posteriori emission fields from the inversion was smaller than that (1.55 ppb) using the a priori field; the mean bias (1.06 ppb) between the observations and simulated mixing ratios using a posteriori emission fields was also smaller than that (1.12 ppb) using the a priori field. Both the RMSEs and mean bias suggest that the a posteriori emissions are more accurate than the a priori emissions.

We also made FLEXPART simulations driven by operational meteorological analyses from the European Centre for Medium-Range Weather Forecasts (ECMWF) instead of CFSR data. The a posteriori emissions for the PRD are very similar when using the emission sensitivities from the two alternative FLEXPART simulations – e.g., for benzene we

not passed over the strong emission sources in the central part of PRD and HK (see the backward emission sensitivities map in Fig. 3c), while the toluene mixing ratio at 00:00 UTC on 24 November 2010 was about 16 ppb and the corresponding air mass had passed over the strong emission sources in the central part of PRD and HK (Fig. 3d).

Figure 4 shows the benzene a priori and a posteriori emission fields, their differences and uncertainty reduction. The a priori fields show that emission hot spots are located in the megacities Guangzhou, Shenzhen, and Hong Kong. Emission changes by the inversion are positive in some grid cells and negative in some other grid cells, which shows that the a priori emissions are not systematically lower or higher everywhere than the a posteriori emissions. The biggest emission changes by the inversion occur in two boxes in Guangzhou where the a priori emissions were enhanced by ∼ 50 % in one box and decreased by more than 50 % in the other box. The emission hot spot in Shenzhen did not change much. To test the sensitivity to the a priori emission in this grid cell, we performed an additional inversion in which the a priori emission in this grid cell was reduced, and a high a posteriori

Figure 4. Maps of **(a)** a priori benzene emissions, **(b)** a posteriori benzene emissions, **(c)** differences between **(b)** and **(a)**, and **(d)** uncertainty reduction. The Heshan observation site is marked with a green cross.
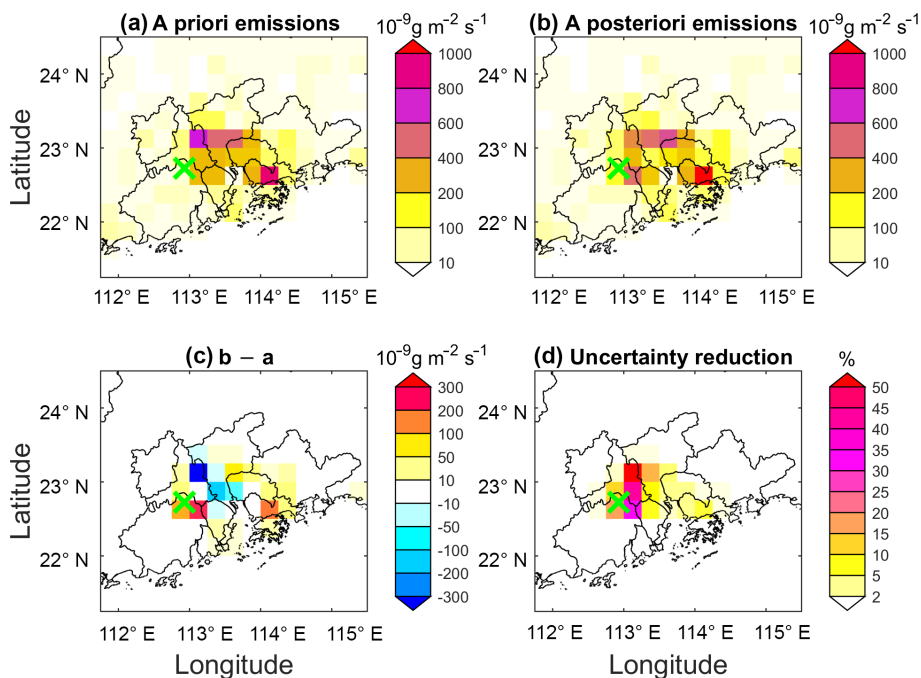

Figure 5. Maps of **(a)** a priori toluene emissions, **(b)** a posteriori toluene emissions, **(c)** differences between **(b)** and **(a)**, and **(d)** uncertainty reduction. The Heshan observation site is marked with a green cross.

obtained $4.0\,\mathrm{Gg\,month^{-1}}$ from the inversion using CFSR and $4.2\,\mathrm{Gg\,month^{-1}}$ from the inversion using ECMWF. Although Fang et al. (2014) showed that FLEXPART simulations driven with ECMWF data performed slightly better

than the CFSR-driven simulations for SF_6 in East Asia for Hateruma, Gosan and Cape Ochiishi stations, we found that CFSR-driven FLEXPART simulations performed slightly better than the ECMWF-driven simulations for the benzene
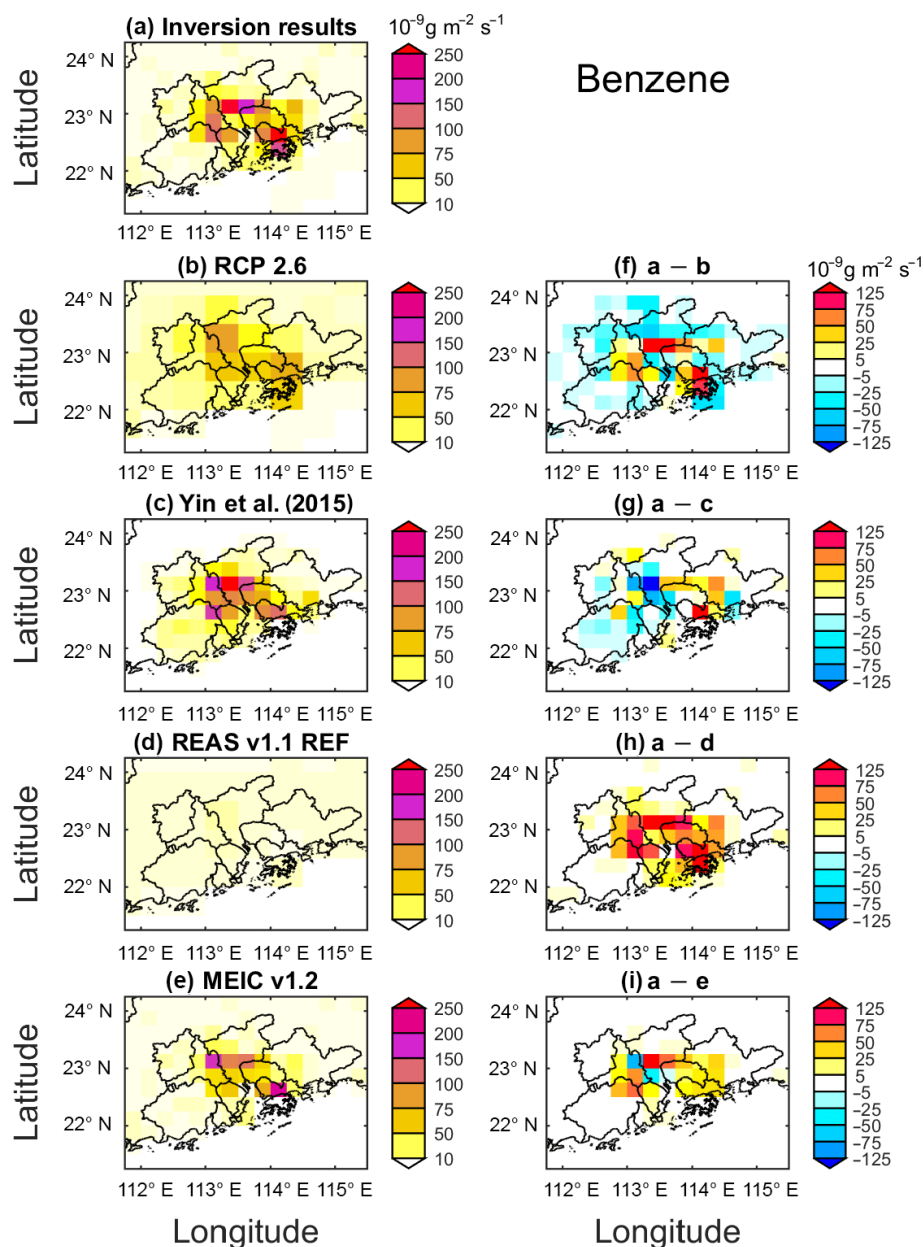
Figure 6. Maps of benzene emissions for the PRD, HK, and surrounding regions from **(a)** inversion, **(b)** RCP2.6, **(c)** Yin et al. (2015), **(d)** REAS v1.1 REF, **(e)** MEIC v1.2, and the difference between inversion results **(a)** and the bottom-up inventories **(b, c, d, e)**. Note that in **(c)** and **(g)** only emissions within the PRD are plotted since Yin et al. (2015) only estimated emissions within PRD, and that in **(e)** and **(i)** emissions within HK are not plotted since MEIC v1.2 has not estimated benzene emissions in HK.

simulations at the Heshan site. Thus, the CFSR data set was used in this paper.

3.4 Comparison with other estimates

Figures 6 and S9, respectively, show spatial distributions of benzene and toluene emissions estimated by the inversion in this study, four bottom-up inventories, and the differences among these estimates. For benzene, the spatial emission distributions in the REAS v1.1 REF have the biggest differ-

ence from our top-down emissions. Gridded emissions in the REAS v1.1 REF are always lower than the inversion emissions, while emissions in the Yin et al. (2015), MEIC v1.2, and RCP2.6 estimates are less systematically biased. The simulated benzene mixing ratios using the REAS v1.1 inventory are much lower than the observed mixing ratios (Fig. 7). Statistics of the RMSE, mean bias, and squared Pearson correlation coefficients between the simulated and observed mixing ratios show that emission fields obtained from the in-
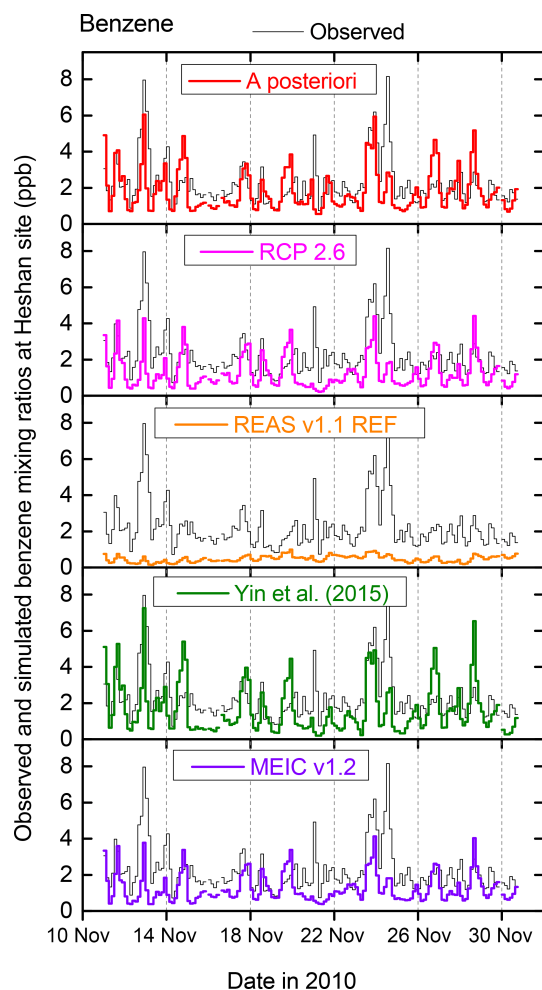
Figure 7. Time series of observed and simulated benzene mixing ratios at the Heshan site. The simulations use emission fields from inversion in this study, RCP2.6, REAS v1.1 REF, Yin et al. (2015), and MEIC v1.2, respectively.

version performed better in simulating the benzene mixing ratios than all four bottom-up inventories (see Table S2).

For toluene, in most grid cells over the PRD, emissions estimated by RCP2.6, Yin et al. (2015), and REAS v1.1 REF are lower than the inversion estimates, while MEIC v1.2 emissions are higher than the inversion estimates (Fig. S9). Model simulations show that the simulated mixing ratios using emission estimates from RCP2.6, Yin et al. (2015), and REAS v1.1 REF are much lower than the observed mixing ratios at the Heshan site (Fig. S10). The simulated mixing ratios using MEIC v1.2 emission fields are not consistent with some observed pollution peaks (Fig. S10). Statistics of RMSE and squared Pearson correlation coefficients show that inversion emission fields performed better at simulating toluene mixing ratios at the Heshan site than the four bottom-up emission fields (see Table S2).

Table 2 shows five estimates of total benzene and toluene emissions in the PRD and HK regions for the year 2010. The a posteriori emissions for November 2010 obtained from the inversion were extrapolated to an annual mean emission rate for the whole year 2010 by multiplying the November emissions by the ratio of emissions for the whole year 2010 to those in November 2010. For toluene, this ratio is 10.8, and was calculated from both the MEIC v1.2 and Yin et al. (2015) estimate (the November/annual emission ratio was the same in both data sets). For toluene, the factor is 10.9 (10.4–11.4), and is the average of 10.4, calculated from the MEIC v1.2 estimate, and 11.4, calculated from the Yin et al. (2015) estimate. Data in November 2010 and the whole year 2010 were obtained through personal communication with the authors of the data set. Using these ratios, the benzene emissions in the PRD and HK for 2010 were estimated to be 44 (12–75) and 5 (2–7) Gg yr^{-1}, respectively, and the toluene emissions were estimated to be 131 (44–218) and 6 (2–9) Gg yr^{-1}, respectively.

For benzene, emissions in the PRD in 2010 calculated from the four bottom-up estimates were 45 Gg yr^{-1} from RCP2.6 (van Vuuren et al., 2007), 54 Gg yr^{-1} from Yin et al. (2015), 8 Gg yr^{-1} from REAS v1.1 REF (Ohara et al., 2007), and 33 Gg yr^{-1} from MEIC v1.2. Our inverse estimate agrees within its uncertainties with these bottom-up estimates, except that the REAS estimate is substantially lower than the other bottom-up and the top-down estimates. Emissions in HK were 5 (2–7) Gg yr^{-1} estimated by this study, which agrees within uncertainties with the RCP2.6 estimate and is much higher than the REAS v1.1 REF (no estimates are available from MEIC v1.2 or Yin et al., 2015).

For toluene, emissions in PRD in 2010 calculated from the four bottom-up estimates were 44 Gg yr^{-1} from RCP2.6 estimate (van Vuuren et al., 2007), 64 Gg yr^{-1} from Yin et al. (2015), 46 Gg yr^{-1} from REAS v1.1 REF (Ohara et al., 2007), and 181 Gg yr^{-1} from MEIC v1.2. The bottom-up estimate MEIC v1.2 meets the high uncertainty range of our inversion estimates, while the other three bottom-up estimates meet the low uncertainty range of our inversion estimates. For the HK toluene emissions, estimates are not available in MEIC v1.2 or Yin et al. (2015); both RCP2.6 and REAS v1.1 REF estimates are about 4 Gg yr^{-1}, which agree with our inversion results within uncertainties.

3.5 Benzene and toluene emissions during 2000–2010

Figure 8 shows different estimates of benzene and toluene emissions in the PRD region for the period 2000–2010. For benzene, the estimate of 8 Gg yr^{-1} in 2000 by REAS v2.1 (Kurokawa et al., 2013) agrees with that of 13 Gg yr^{-1} by the Reanalysis of the Tropospheric chemical composition over the past 40 years project (RETRO) (Schultz et al., 2007), which are substantially smaller than that of 43 Gg yr^{-1} in the Atmospheric Chemistry and Climate Model Intercomparison Project (ACCMIP) (Lamarque et al., 2010). For
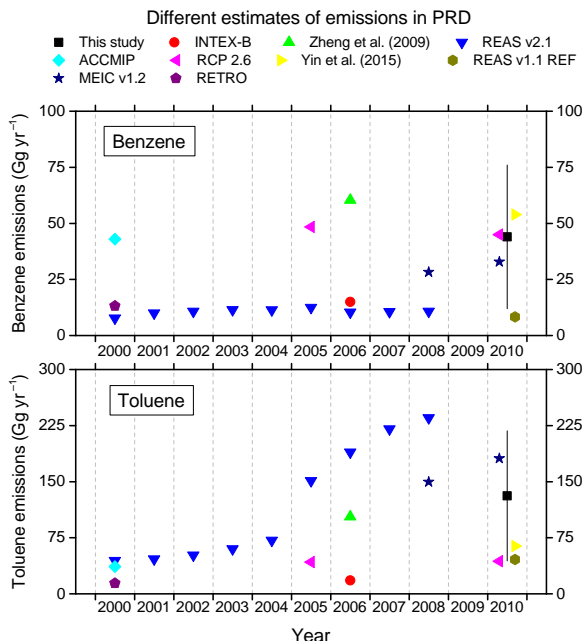
Figure 8. Estimates of benzene and toluene emissions in the PRD region for the period 2000–2010.

the years 2005 and 2006, different studies show substantial differences. For the year 2005, the emission estimate by RCP2.6 was ~ 4 times the estimates by REAS v2.1. For the year 2006, the emission estimate by REAS v2.1 agrees with the estimate in the Intercontinental Chemical Transport Experiment Phase B (INTEX-B) project (Zhang et al., 2009), which were only $\sim 20\%$ of the estimate by Zheng et al. (2009). More studies are available for the year 2010 than for other years. For the year 2010, the estimates by RCP2.6, MEIC v1.2, and Yin et al. (2015) agree with the inversion estimate by this study, which are higher than the estimate by REAS v1.1 REF. According to these bottom-up and top-down estimates (Fig. 8), it is likely that the benzene emissions in the PRD have remained relatively stable during the 2000–2010 period, although emissions are uncertain due to the limited number of estimates.

For toluene, the estimate of $45\,\mathrm{Gg\,yr^{-1}}$ in 2000 by REAS v2.1 (Kurokawa et al., 2013) agrees relatively well with the value of $36\,\mathrm{Gg\,yr^{-1}}$ by ACCMIP (Lamarque et al., 2010), but both are substantially larger than the RETRO estimate of $14\,\mathrm{Gg\,yr^{-1}}$ (Schultz et al., 2007). For the years 2005 and 2006, estimates of toluene emission are also quite different. For the year 2005, the emission estimate by REAS v2.1 was ~ 4 times the estimates by RCP2.6. For the year 2006, the emission estimate by REAS v2.1 was ~ 2 times the estimate by Zheng et al. (2009) and even ~ 11 times the estimate by INTEX-B (Zhang et al., 2009). For the year 2010, the estimates by REAS v1.1 REF and Yin et al. (2015) meet the

low end of uncertainty of inversion estimate by this study, while the MEIC v1.2 estimate meets the high end. According to these estimates over 2000–2010 (Fig. 8), it is likely that the toluene emissions in the PRD have increased during this period, although emissions are uncertain due to the limited number of estimates.

Based on glyoxal (CHOCHO) data retrieved from satellite and inversion method, Liu et al. (2012) found that their emission estimates of the lumped artificial compound ARO1 (benzene, toluene, and ethylbenzene) in the PRD in 2006 were >10 times larger than the bottom-up INTEX-B estimates (also for 2006), but they did not specify which compound was responsible for the difference. As for benzene, the ratio of emissions in 2006 estimated by Zheng et al. (2009) ($60\,\mathrm{Gg\,yr^{-1}}$) to the INTEX-B estimate ($15\,\mathrm{Gg\,yr^{-1}}$) is ~ 4 times, much less than the factor > 10 discrepancy reported by Liu et al. (2012). Inversion estimate of benzene emissions ($44\,(12$–$75)\,\mathrm{Gg\,yr^{-1}}$) in 2010 is $\sim 3\,(1$–$5)$ times the INTEX-B emissions for 2006. Thus, we suggest that the big discrepancy is likely not due to emissions of benzene but emissions of toluene and/or ethylbenzene. As for toluene emissions, the ratios of bottom-up estimates by REAS v2.1 ($190\,\mathrm{Gg\,yr^{-1}}$) and Zheng et al. (2009) ($103\,\mathrm{Gg\,yr^{-1}}$) for 2006 to the INTEX-B bottom-up estimate for 2006 ($18\,\mathrm{Gg\,yr^{-1}}$) are 11–6. Thus, considering the satellite-based estimate and other bottom-up estimates, the bottom-up INTEX-B estimate of toluene emissions for the PRD region for 2006 was likely too low, and estimation of toluene emissions in the PRD is attributed as an important factor contributing to the big discrepancy of ARO1 emission estimates between Liu et al. (2012) and INTEX-B.

3.6 Suggestions for more top-down studies

To the best of our knowledge, this study provides the only available top-down estimate for benzene and toluene emissions in the PRD and HK regions. All other studies in Fig. 8 are bottom-up estimates. More top-down estimates are needed to validate the bottom-up estimates in previous years and in the future. In this study, inversions using the Heshan measurement data reduced emission uncertainties in the PRD and HK regions. However, the emission uncertainty reductions were not large because there was only one observation site suitable for the inversion (some measurements in urban environments are available but not suitable for inverse modeling) and the observation period was not long. Thus, we propose that in the future, observations with better spatial and temporal coverage are urgently needed to better constrain benzene and toluene (and other VOC) emissions in the PRD and HK regions. Inversion-suited observation sites could be situated in rural places outside of the major emission sources located in the central part of PRD and HK regions, and then the major emission sources in the PRD and HK regions could be "viewed" from different angles (multiple-site

inversion) to better constrain the benzene and toluene (and other VOC) emissions.

4   Conclusions

Using atmospheric measurements at the Heshan site, a transport model, and an inversion algorithm, this study provides the first top-down estimate of benzene and toluene emissions in the Pearl River Delta (PRD) and Hong Kong (HK) regions, which are emission hot spots in China. According to the measurement data in this study and previous studies, mixing ratio levels of benzene and toluene in the PRD region are overall higher than those in Hong Kong, which are much higher than those measured in the United States and Europe. Considering that air masses transported to the Heshan site mainly came from easterly and northerly directions during the observation period, and that the major emissions sources in the PRD are located to the east of the Heshan site, the Heshan measurement site was ideally situated for constraining emissions from these regions. Based on the measurement data, model simulations, and inverse technique, the PRD and HK benzene emissions for 2010 estimated in this study were $44\,(12\text{–}75)$ and $5\,(2\text{–}7)\,\mathrm{Gg\,yr^{-1}}$, respectively and the PRD and HK toluene emissions for 2010 were $131\,(44\text{–}218)$ and $6\,(2\text{–}9)\,\mathrm{Gg\,yr^{-1}}$, respectively. We have discussed the spatial distributions of benzene and toluene emissions obtained by inversion in this study in the context of four different existing bottom-up inventories. The discrepancies among these bottom-up estimates for the period 2000–2010 are substantial (up to a factor of seven), while this study is the only available top-down estimate. We propose that observations with better spatial and temporal coverage are urgently needed to constrain benzene and toluene (and other VOC) emissions in the PRD and HK regions more strongly.

The Supplement related to this article is available online at doi:10.5194/acp-16-3369-2016-supplement.

References

Ait-Helal, W., Borbon, A., Sauvage, S., de Gouw, J. A., Colomb, A., Gros, V., Freutel, F., Crippa, M., Afif, C., Baltensperger, U., Beekmann, M., Doussin, J. F., Durand-Jolibois, R., Fronval, I., Grand, N., Leonardis, T., Lopez, M., Michoud, V., Miet, K., Perrier, S., Prévôt, A. S. H., Schneider, J., Siour, G., Zapf, P., and Locoge, N.: Volatile and intermediate volatility organic compounds in suburban Paris: variability, origin and importance for SOA formation, Atmos. Chem. Phys., 14, 10439–10464, doi:10.5194/acp-14-10439-2014, 2014.

Baker, A. K., Beyersdorf, A. J., Doezema, L. A., Katzenstein, A., Meinardi, S., Simpson, I. J., Blake, D. R., and Sherwood Rowland, F.: Measurements of nonmethane hydrocarbons in 28 United States cities, Atmos. Environ., 42, 170–182, 2008.

Barletta, B., Meinardi, S., Simpson, I. J., Khwaja, H. A., Blake, D. R., and Rowland, F. S.: Mixing ratios of volatile organic compounds (VOCs) in the atmosphere of Karachi, Pakistan, Atmos. Environ., 36, 3429–3443, 2002.

Barletta, B., Meinardi, S., Rowland, F. S., Chan, C. Y., Wang, X. M., Zou, S. C., Chan, L. Y., and Blake, D. R.: Volatile organic compounds in 43 Chinese cities, Atmos. Environ., 39, 5979–5990, 2005.

Barletta, B., Meinardi, S., Simpson, I. J., Zou, S., Sherwood Rowland, F., and Blake, D. R.: Ambient mixing ratios of nonmethane hydrocarbons (NMHCs) in two major urban centers of the Pearl River Delta (PRD) region: Guangzhou and Dongguan, Atmos. Environ., 42, 4393–4408, 2008.

Chan, L.-Y., Chu, K.-W., Zou, S.-C., Chan, C.-Y., Wang, X.-M., Barletta, B., Blake, D. R., Guo, H., and Tsai, W.-Y.: Characteristics of nonmethane hydrocarbons (NMHCs) in industrial, industrial-urban, and industrial-suburban atmospheres of the Pearl River Delta (PRD) region of south China, J. Geophys. Res.-Atmos., 111, D11304, doi:10.1029/2005JD006481, 2006.

Donald, J. M., Hooper, K., and Hopenhayn-Rich, C.: Reproductive and Developmental Toxicity of Toluene: A Review, Environ. Health Perspect., 94, 237–244, doi:10.2307/3431317, 1991.

Fang, X., Thompson, R. L., Saito, T., Yokouchi, Y., Kim, J., Li, S., Kim, K. R., Park, S., Graziosi, F., and Stohl, A.: Sulfur hexafluoride (SF_6) emissions in East Asia determined by inverse modeling, Atmos. Chem. Phys., 14, 4779–4791, doi:10.5194/acp-14-4779-2014, 2014.

Fang, X., Stohl, A., Yokouchi, Y., Kim, J., Li, S., Saito, T., Park, S., and Hu, J.: Multiannual Top-Down Estimate of HFC-23 Emissions in East Asia, Environ. Sci. Technol., 49, 4345–4353, doi:10.1021/es505669j, 2015.

Guo, H., Jiang, F., Cheng, H. R., Simpson, I. J., Wang, X. M., Ding, A. J., Wang, T. J., Saunders, S. M., Wang, T., Lam, S. H. M., Blake, D. R., Zhang, Y. L., and Xie, M.: Concurrent observations of air pollutants at two sites in the Pearl River Delta and the implication of regional transport, Atmos. Chem. Phys., 9, 7343–7360, doi:10.5194/acp-9-7343-2009, 2009.

Guo, H., Ling, Z. H., Cheung, K., Jiang, F., Wang, D. W., Simpson, I. J., Barletta, B., Meinardi, S., Wang, T. J., Wang, X. M., Saunders, S. M., and Blake, D. R.: Characterization of photochemical pollution at different elevations in mountainous areas in Hong Kong, Atmos. Chem. Phys., 13, 3881–3898, doi:10.5194/acp-13-3881-2013, 2013.

Guo, S., Hu, M., Zamora, M. L., Peng, J., Shang, D., Zheng, J., Du, Z., Wu, Z., Shao, M., Zeng, L., Molina, M. J., and Zhang, R.: Elu-

cidating severe urban haze formation in China, P. Natl. Acad. Sci. USA, 111, 17373–17378, doi:10.1073/pnas.1419604111, 2014.

Henze, D. K., Seinfeld, J. H., Ng, N. L., Kroll, J. H., Fu, T. M., Jacob, D. J., and Heald, C. L.: Global modeling of secondary organic aerosol formation from aromatic hydrocarbons: high-vs. low-yield pathways, Atmos. Chem. Phys., 8, 2405–2420, doi:10.5194/acp-8-2405-2008, 2008.

Kurokawa, J., Ohara, T., Morikawa, T., Hanayama, S., Janssens-Maenhout, G., Fukui, T., Kawashima, K., and Akimoto, H.: Emissions of air pollutants and greenhouse gases over Asian regions during 2000–2008: Regional Emission inventory in ASia (REAS) version 2, Atmos. Chem. Phys., 13, 11019–11058, doi:10.5194/acp-13-11019-2013, 2013.

Lamarque, J. F., Bond, T. C., Eyring, V., Granier, C., Heil, A., Klimont, Z., Lee, D., Liousse, C., Mieville, A., Owen, B., Schultz, M. G., Shindell, D., Smith, S. J., Stehfest, E., Van Aardenne, J., Cooper, O. R., Kainuma, M., Mahowald, N., McConnell, J. R., Naik, V., Riahi, K., and van Vuuren, D. P.: Historical (1850–2000) gridded anthropogenic and biomass burning emissions of reactive gases and aerosols: methodology and application, Atmos. Chem. Phys., 10, 7017–7039, doi:10.5194/acp-10-7017-2010, 2010.

Langford, B., Nemitz, E., House, E., Phillips, G. J., Famulari, D., Davison, B., Hopkins, J. R., Lewis, A. C., and Hewitt, C. N.: Fluxes and concentrations of volatile organic compounds above central London, UK, Atmos. Chem. Phys., 10, 627–645, doi:10.5194/acp-10-627-2010, 2010.

Lau, A. K. H., Yuan, Z., Yu, J. Z., and Louie, P. K. K.: Source apportionment of ambient volatile organic compounds in Hong Kong, Sci. Total Environ., 408, 4138–4149, 2010.

Liu, Y., Shao, M., Lu, S., Chang, C.-c., Wang, J.-L., and Chen, G.: Volatile Organic Compound (VOC) measurements in the Pearl River Delta (PRD) region, China, Atmos. Chem. Phys., 8, 1531–1545, doi:10.5194/acp-8-1531-2008, 2008.

Liu, Z., Wang, Y. H., Vrekoussis, M., Richter, A., Wittrock, F., Burrows, J. P., Shao, M., Chang, C. C., Liu, S. C., Wang, H. L., and Chen, C. H.: Exploring the missing source of glyoxal (CHOCHO) over China, Geophys. Res. Lett., 39, L10812, doi:10.1029/2012gl051645, 2012.

Ohara, T., Akimoto, H., Kurokawa, J., Horii, N., Yamaji, K., Yan, X., and Hayasaka, T.: An Asian emission inventory of anthropogenic emission sources for the period 1980–2020, Atmos. Chem. Phys., 7, 4419–4444, doi:10.5194/acp-7-4419-2007, 2007.

Ou, J., Zheng, J., Li, R., Huang, X., Zhong, Z., Zhong, L., and Lin, H.: Speciated OVOC and VOC emission inventories and their implications for reactivity-based ozone control strategy in the Pearl River Delta region, China, Sci. Total Environ., 530–531, 393–402, 2015.

Ran, L., Zhao, C., Geng, F., Tie, X., Tang, X., Peng, L., Zhou, G., Yu, Q., Xu, J., and Guenther, A.: Ozone photochemical production in urban Shanghai, China: Analysis based on ground level observations, J. Geophys. Res.-Atmos., 114, D15301, doi:10.1029/2008JD010752, 2009.

Saha, S., Moorthi, S., Pan, H.-L., Wu, X., Wang, J., Nadiga, S., Tripp, P., Kistler, R., Woollen, J., Behringer, D., Liu, H., Stokes, D., Grumbine, R., Gayno, G., Wang, J., Hou, Y.-T., Chuang, H.-Y., Juang, H.-M. H., Sela, J., Iredell, M., Treadon, R., Kleist, D., Van Delst, P., Keyser, D., Derber, J., Ek, M., Meng, J., Wei,

H., Yang, R., Lord, S., van den Dool, H., Kumar, A., Wang, W., Long, C., Chelliah, M., Xue, Y., Huang, B., Schemm, J.-K., Ebisuzaki, W., Lin, R., Xie, P., Chen, M., Zhou, S., Higgins, W., Zou, C.-Z., Liu, Q., Chen, Y., Han, Y., Cucurull, L., Reynolds, R. W., Rutledge, G., and Goldberg, M.: NCEP Climate Forecast System Reanalysis (CFSR) 6-hourly Products, January 1979 to December 2010, Research Data Archive at the National Center for Atmospheric Research, Computational and Information Systems Laboratory, Boulder, CO, 2010.

Schultz, M., Rast, S., van het Bolscher, M., Pulles, T., Brand, R., Pereira, J., Mota, B., Spessa, A., Dalsøren, S., van Nojie, T., and Szopa, S.: Emission data sets and methodologies for estimating emissions, RETRO project report D1-6, Hamburg, http://retro-archive.iek.fz-juelich.de/data/documents/reports/D1-6_final.pdf (last access: 10 March 2016), 2007.

Seibert, P. and Frank, A.: Source-receptor matrix calculation with a Lagrangian particle dispersion model in backward mode, Atmos. Chem. Phys., 4, 51–63, doi:10.5194/acp-4-51-2004, 2004.

Seibert, P., Kristiansen, N. I., Richter, A., Eckhardt, S., Prata, A. J., and Stohl, A.: Uncertainties in the inverse modelling of sulphur dioxide eruption profiles, Geomat. Nat. Hazards Risk, 2, 201–216, doi:10.1080/19475705.2011.590533, 2011.

Seila, R. L., Lonneman, W. A., Meeks, S. A., and Atmospheric Research and Exposure Assessment Laboratory (U.S.): Determination of C2 to C12 ambient air hydrocarbons in 39 U.S. cities, from 1984 though 1986, EPA/600/S3-89/058, Research Triangle Park, NC, US Environmental Protection Agency, Atmospheric Research and Exposure Assessment Laboratory, 1989.

Simpson, I. J., Blake, N. J., Barletta, B., Diskin, G. S., Fuelberg, H. E., Gorham, K., Huey, L. G., Meinardi, S., Rowland, F. S., Vay, S. A., Weinheimer, A. J., Yang, M., and Blake, D. R.: Characterization of trace gases measured over Alberta oil sands mining operations: 76 speciated C_2–C_{10} volatile organic compounds (VOCs), CO_2, CH_4, CO, NO, NO_2, NO_y, O_3 and SO_2, Atmos. Chem. Phys., 10, 11931–11954, doi:10.5194/acp-10-11931-2010, 2010.

Song, Y., Shao, M., Liu, Y., Lu, S., Kuster, W., Goldan, P., and Xie, S.: Source Apportionment of Ambient Volatile Organic Compounds in Beijing, Environ. Sci. Technol., 41, 4348–4353, doi:10.1021/es0625982, 2007.

Stohl, A. and Thomson, D.: A Density Correction for Lagrangian Particle Dispersion Models, Bound.-Lay. Meteorol., 90, 155–167, doi:10.1023/A:1001741110696, 1999.

Stohl, A., Hittenberger, M., and Wotawa, G.: Validation of the Lagrangian particle dispersion model FLEXPART against large-scale tracer experiment data, Atmos. Environ., 32, 4245–4264, 1998.

Stohl, A., Forster, C., Frank, A., Seibert, P., and Wotawa, G.: Technical note: The Lagrangian particle dispersion model FLEXPART version 6.2, Atmos. Chem. Phys., 5, 2461–2474, doi:10.5194/acp-5-2461-2005, 2005.

Stohl, A., Seibert, P., Arduini, J., Eckhardt, S., Fraser, P., Greally, B. R., Lunder, C., Maione, M., Mühle, J., O'Doherty, S., Prinn, R. G., Reimann, S., Saito, T., Schmidbauer, N., Simmonds, P. G., Vollmer, M. K., Weiss, R. F., and Yokouchi, Y.: An analytical inversion method for determining regional and global emissions of greenhouse gases: Sensitivity studies and application to halocarbons, Atmos. Chem. Phys., 9, 1597–1620, doi:10.5194/acp-9-1597-2009, 2009.

Stohl, A., Kim, J., Li, S., O'Doherty, S., Mühle, J., Salameh, P. K., Saito, T., Vollmer, M. K., Wan, D., Weiss, R. F., Yao, B., Yokouchi, Y., and Zhou, L. X.: Hydrochlorofluorocarbon and hydrofluorocarbon emissions in East Asia determined by inverse modeling, Atmos. Chem. Phys., 10, 3545–3560, doi:10.5194/acp-10-3545-2010, 2010.

van Donkelaar, A., Martin, R. V., Brauer, M., Kahn, R., Levy, R., Verduzco, C., and Villeneuve, P. J.: Global Estimates of Ambient Fine Particulate Matter Concentrations from Satellite-Based Aerosol Optical Depth: Development and Application, Environ. Health Perspect., 118, 847–855, 2010.

van Vuuren, D., den Elzen, M. J., Lucas, P., Eickhout, B., Strengers, B., van Ruijven, B., Wonink, S., and van Houdt, R.: Stabilizing greenhouse gas concentrations at low levels: an assessment of reduction strategies and costs, Climatic Change, 81, 119–159, doi:10.1007/s10584-006-9172-9, 2007.

Velasco, E., Lamb, B., Westberg, H., Allwine, E., Sosa, G., Arriaga-Colina, J. L., Jobson, B. T., Alexander, M. L., Prazeller, P., Knighton, W. B., Rogers, T. M., Grutter, M., Herndon, S. C., Kolb, C. E., Zavala, M., de Foy, B., Volkamer, R., Molina, L. T., and Molina, M. J.: Distribution, magnitudes, reactivities, ratios and diurnal patterns of volatile organic compounds in the Valley of Mexico during the MCMA 2002 & 2003 field campaigns, Atmos. Chem. Phys., 7, 329–353, doi:10.5194/acp-7-329-2007, 2007.

Wang, M., Zeng, L., Lu, S., Shao, M., Liu, X., Yu, X., Chen, W., Yuan, B., Zhang, Q., Hu, M., and Zhang, Z.: Development and validation of a cryogen-free automatic gas chromatograph system (GC-MS/FID) for online measurements of volatile organic compounds, Anal. Methods, 6, 9424–9434, doi:10.1039/C4AY01855A, 2014.

Weiss, R. F. and Prinn, R. G.: Quantifying greenhouse-gas emissions from atmospheric measurements: a critical reality check for climate legislation, Philos. T. Roy. Soc. A, 369, 1925–1942, doi:10.1098/rsta.2011.0006, 2011.

White, M. L., Russo, R. S., Zhou, Y., Ambrose, J. L., Haase, K., Frinak, E. K., Varner, R. K., Wingenter, O. W., Mao, H., Talbot, R., and Sive, B. C.: Are biogenic emissions a significant source of summertime atmospheric toluene in the rural Northeastern United States?, Atmos. Chem. Phys., 9, 81–92, doi:10.5194/acp-9-81-2009, 2009.

Xue, L. K., Wang, T., Gao, J., Ding, A. J., Zhou, X. H., Blake, D. R., Wang, X. F., Saunders, S. M., Fan, S. J., Zuo, H. C., Zhang, Q. Z., and Wang, W. X.: Ground-level ozone in four Chinese cities: precursors, regional transport and heterogeneous processes, Atmos. Chem. Phys., 14, 13175–13188, doi:10.5194/acp-14-13175-2014, 2014.

Yin, S., Zheng, J., Lu, Q., Yuan, Z., Huang, Z., Zhong, L., and Lin, H.: A refined 2010-based VOC emission inventory and its improvement on modeling regional ozone in the Pearl River Delta Region, China, Sci. Total Environ., 514, 426–438, 2015.

Yoshino, A., Nakashima, Y., Miyazaki, K., Kato, S., Suthawaree, J., Shimo, N., Matsunaga, S., Chatani, S., Apel, E., Greenberg, J., Guenther, A., Ueno, H., Sasaki, H., Hoshi, J.-Y., Yokota, H., Ishii, K., and Kajii, Y.: Air quality diagnosis from comprehensive observations of total OH reactivity and reactive trace species in urban central Tokyo, Atmos. Environ., 49, 51–59, 2012.

Zhang, Q., Streets, D. G., Carmichael, G. R., He, K. B., Huo, H., Kannari, A., Klimont, Z., Park, I. S., Reddy, S., Fu, J. S., Chen, D., Duan, L., Lei, Y., Wang, L. T., and Yao, Z. L.: Asian emissions in 2006 for the NASA INTEX-B mission, Atmos. Chem. Phys., 9, 5131–5153, doi:10.5194/acp-9-5131-2009, 2009.

Zheng, J., Shao, M., Che, W., Zhang, L., Zhong, L., Zhang, Y., and Streets, D.: Speciated VOC Emission Inventory and Spatial Patterns of Ozone Formation Potential in the Pearl River Delta, China, Environ. Sci. Technol., 43, 8580–8586, doi:10.1021/es901688e, 2009.